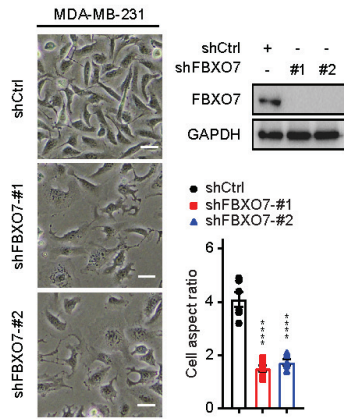
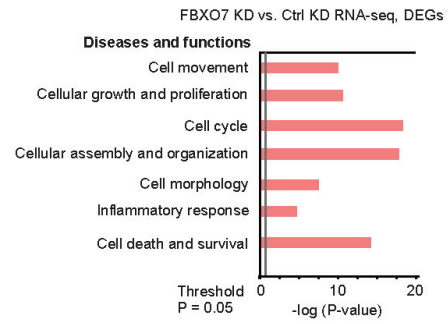


A



B



C

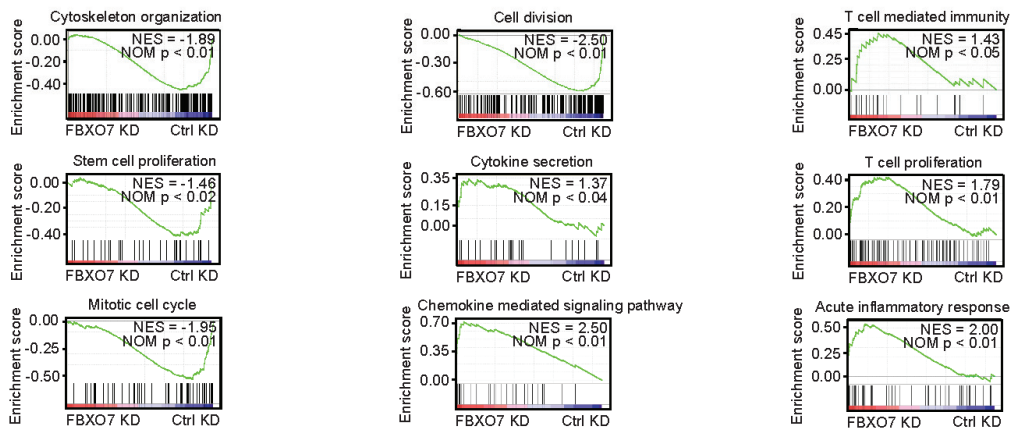


Figure S1. FBXO7 maintains mesenchymal and immune evasion phenotypes of cancer cells, related to Figure 1.

(A) Representative images of control and FBXO7 KD MDA-MB-231 cells (left panels). Scale bar, 10 μ m. Immunoblots of indicated proteins and quantification of cell aspect ratio (right panels). GAPDH, loading control. Six cells from 3 different fields (2 for each) were randomly chosen for each sample (n = 6).

(B) Functional analysis of differentially expressed genes (DEGs) from FBXO7 KD vs. control KD RNA-seq in MDA-MB-231 cells.

(C) GSEA enrichment plots for select gene sets by RNA-seq (FBXO7 KD vs. control KD). NES and p values are shown. Data represent mean \pm SEM. ****p < 0.0001; one-way ANOVA followed by Tukey's multiple comparisons test (A).

Figure S2

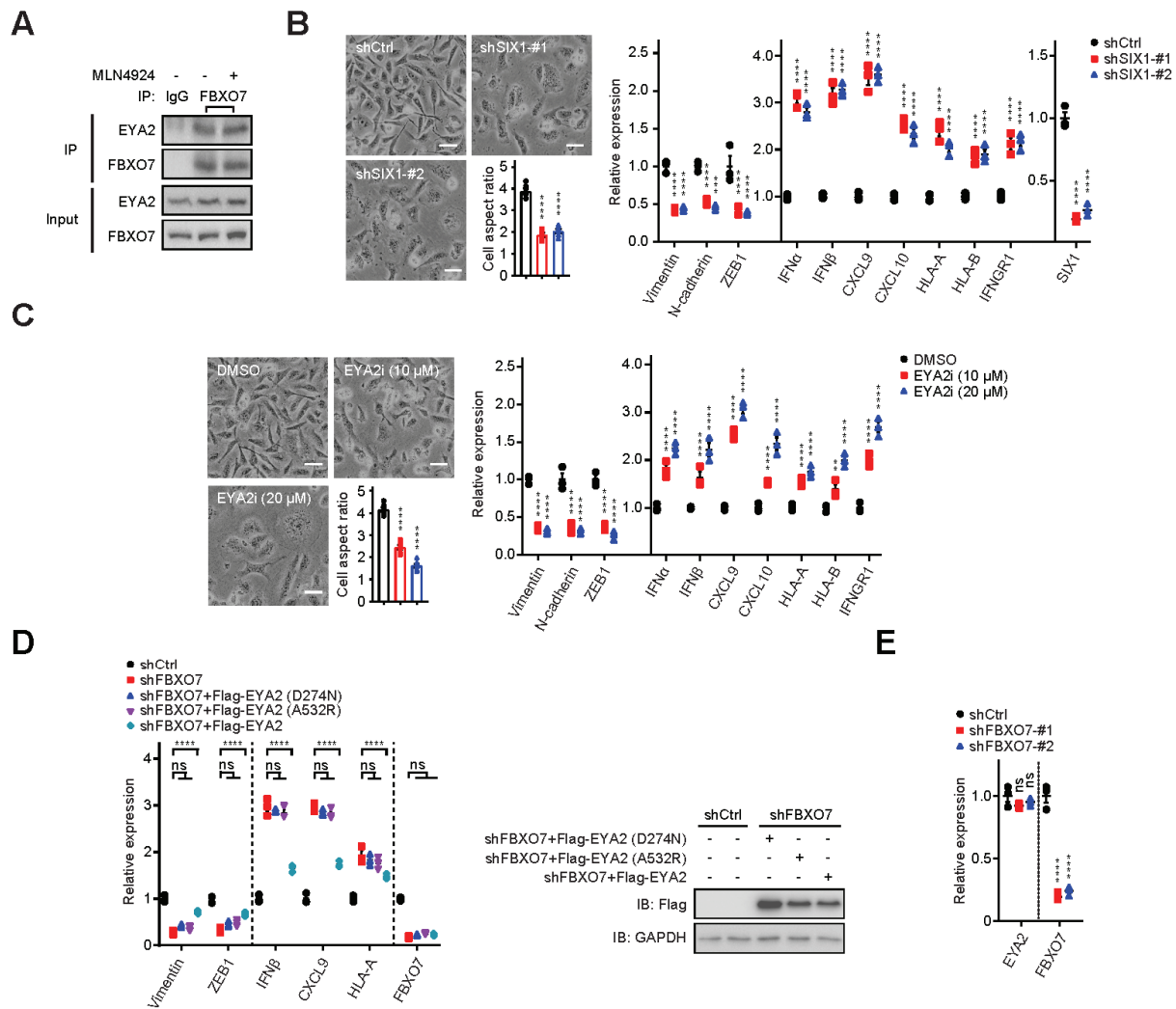


Figure S2. FBXO7 binds and stabilizes SIX1 co-transcriptional regulator EYA2, related to Figure 2.

(A) Co-IP of endogenous FBXO7 with EYA2 in HEK293T cells treated with vehicle or NEDDylation inhibitor MLN4924. IgG, IP control.

(B) Representative images (left panels) and RT-qPCR analysis of the indicated genes (right panel) in control and SIX1 KD MDA-MB-231 cells (n = 3). Scale bar, 100 μ m. Cell aspect ratio (left panel). Six cells from 3 different fields (2 for each) were randomly chosen (n = 6).

(C) Representative images (left panels) and RT-qPCR analysis of the indicated genes (right panel) in vehicle or EYA2i-treated MDA-MB-231 cells (n = 3). Scale bar, 100 μ m. Cell aspect ratio (left panel). Six cells from 3 different fields (2 for each) were randomly chosen (n = 6).

(D) RT-qPCR analysis of the indicated genes in control or FBXO7 KD MDA-MB-231 cells expressing EYA2, EYA2^{D274N}, or EYA2^{A532R} (left panel) (n = 3). Immunoblots of indicated proteins (right panel). GAPDH, loading control.

(E) RT-qPCR analysis of the indicated genes in control or FBXO7 KD MDA-MB-231 cells (n = 3).

Data represent mean \pm SEM. ns, not significant; **p < 0.01; ***p < 0.001; ****p < 0.0001 by one-way ANOVA followed by Tukey's multiple comparisons test (B and C, right panels), and two-way ANOVA followed by Tukey's multiple comparisons test (B and C, left panels; D, and E).

Figure S3

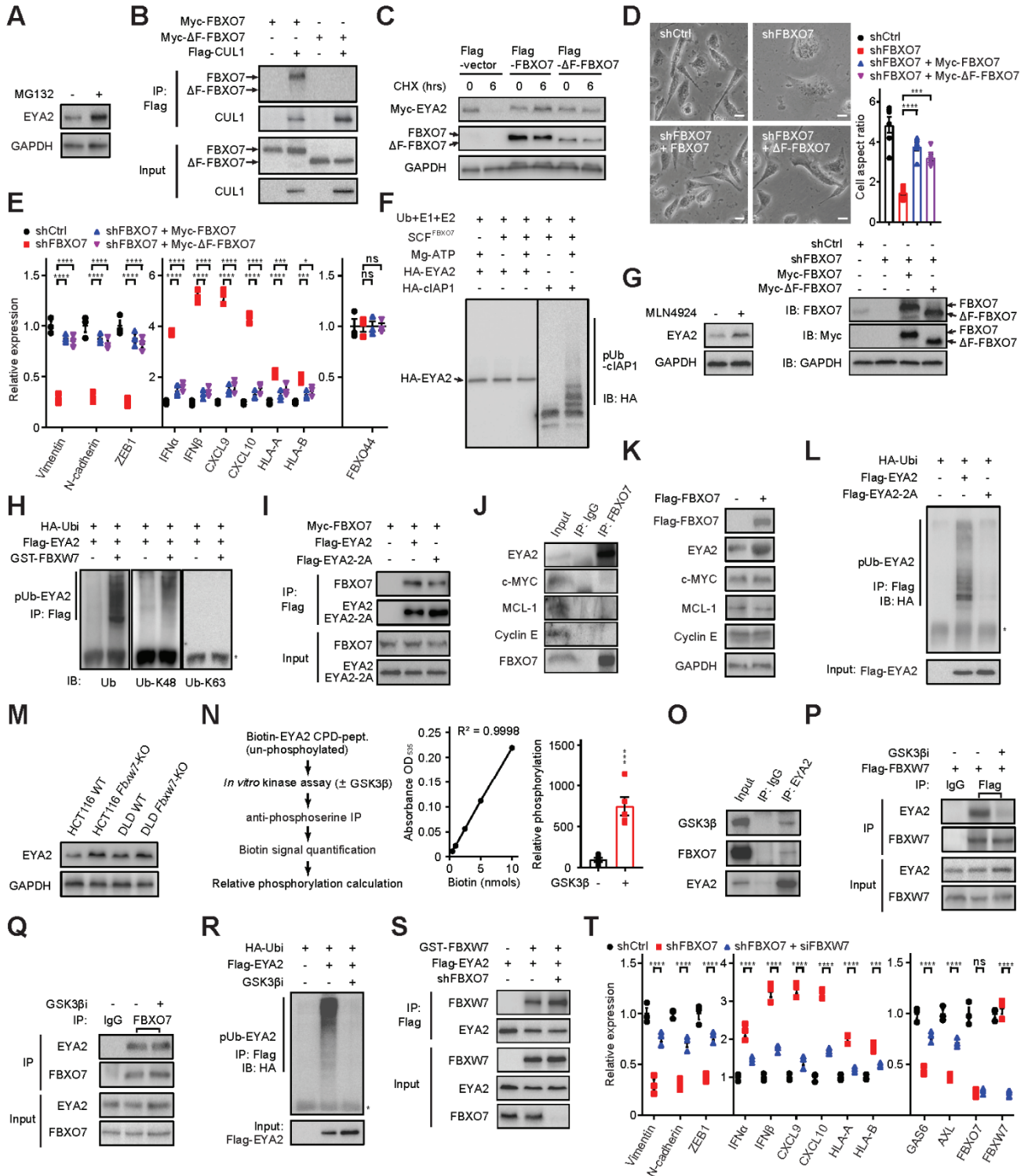


Figure S3. FBXO7 protects EYA2 from SCF^{FBXW7}-dependent degradation, related to Figure 3.

- (A) Immunoblot of EYA2 in HEK293T cells treated with vehicle or 26S proteasome inhibitor MG132. GAPDH, loading control.
- (B) Co-IP of Flag-CUL1 with Myc-FBXO7 or Myc-ΔF-FBXO7 in MDA-MB-231 cells.
- (C) Myc-EYA2 stability in MDA-MB-231 cells expressing control, WT FBXO7, or ΔF-FBXO7. GAPDH, loading control.
- (D) Representative images of control or FBXO7 KD MDA-MB-231 cells expressing Myc-FBXO7 or Myc-ΔF-FBXO7 (left panels). Cell aspect ratio (top right panel). Six cells from 3 different fields (2 for each) were randomly chosen (n = 6). Immunoblots of indicated proteins (bottom right panel). GAPDH, loading control.
- (E) RT-qPCR analysis of the indicated genes in control or FBXO7 KD MDA-MB-231 cells expressing Myc-FBXO7 or Myc-ΔF-FBXO7 (n = 3). FBXO44, control.
- (F) *In vitro* ubiquitylation reactions of SCF^{FBXO7} with HA-EYA2. HA-clAP, positive control.
- (G) Immunoblot of EYA2 in HEK293T cells treated with vehicle or MLN4924. GAPDH, loading control.
- (H) *In vivo* ubiquitylation reactions of HEK293T cells transfected with Flag-EYA2 and GST-FBXW7 vectors and probed with the indicated anti-ubiquitin antibodies. *, IgG heavy chain.
- (I) Co-IP of Flag-EYA2 or Flag-EYA2-2A with Myc-FBXO7 in MDA-MB-231 cells.
- (J) Co-IP of endogenous FBXO7 with EYA2 and known SCF^{FBXW7} substrates in HEK293T cells. IgG, IP control.
- (K) Immunoblots of EYA2 and SCF^{FBXW7} substrates in HEK293T cells expressing control or Flag-FBXO7. GAPDH, loading control.
- (L) *In vivo* ubiquitylation reactions of Flag-EYA2 and Flag-EYA2-2A in HEK293T cells. *, IgG heavy chain.
- (M) Immunoblot of endogenous EYA2 in the indicated WT and *Fbxw7* KO colorectal cancer cells. GAPDH, loading control.
- (N) Schematic (left panel), standard curve (middle panel), and quantification (right panel) of *in vitro* kinase assays for EYA2 CPD peptide incubated with/without recombinant GSK3β (n = 5).
- (O) Co-IP of endogenous EYA2 with GSK3β in HEK293T cells. FBXO7, positive control. IgG, IP control.
- (P and Q) Co-IP of Flag-FBXW7 (P) or endogenous FBXO7 (Q) with EYA2 in HEK293T cells treated with vehicle or GSK3βi. IgG, IP control.
- (R) Immunoblot of pUb Flag-EYA2 in HEK293T cells treated with vehicle or GSK3βi. *, IgG heavy chain.
- (S) Co-IP of Flag-EYA2 with GST-FBXW7 in control and FBXO7 KD MDA-MB-231 cells.
- (T) RT-qPCR analysis of the indicated genes in control, FBXO7 KD, or FBXO7 + FBXW7 KD MDA-MB-231 cells (n = 3).
- Data represent mean ± SEM. ns, not significant; *p < 0.05; ***p < 0.001; ****p < 0.0001 by one-way ANOVA followed by Tukey's multiple comparisons test (D), two-way ANOVA followed by Tukey's multiple comparisons test (E and T), and unpaired Student's *t*-test (N).

Figure S4

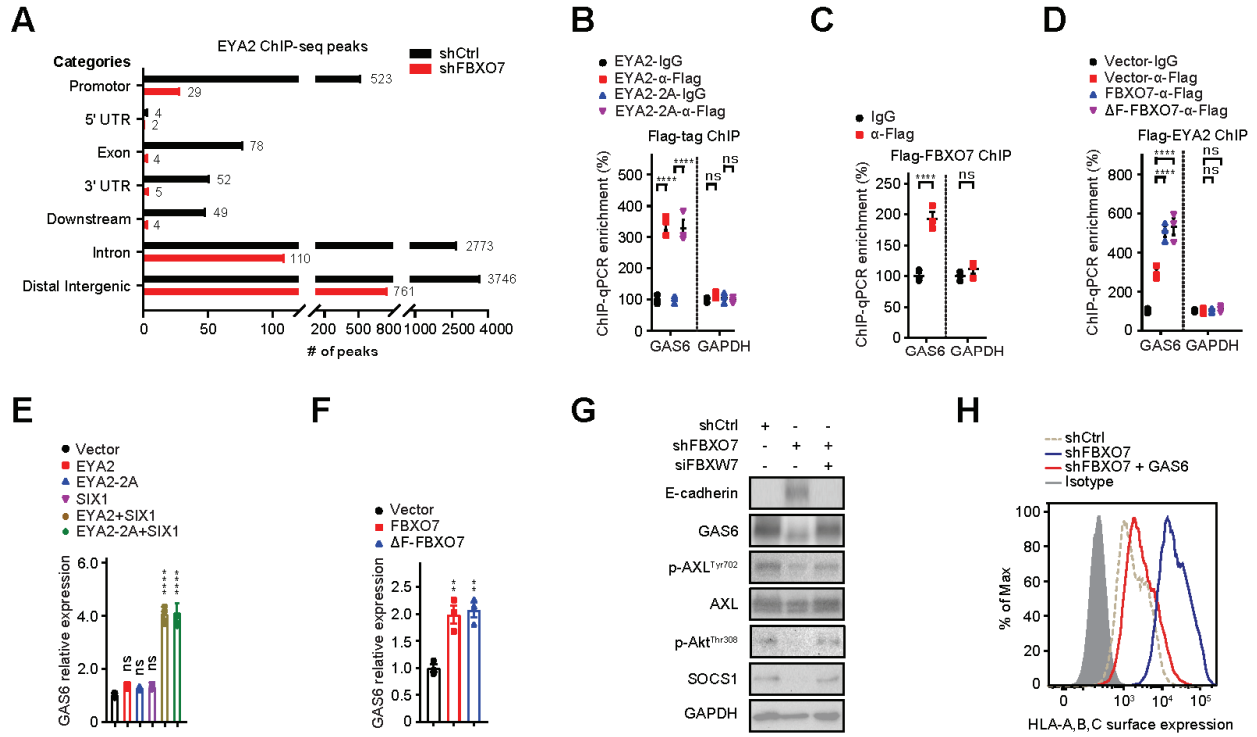


Figure S4. FBXO7 promotes EYA2/SIX1-mediated induction of AXL ligand GAS6, related to Figure 4.

(A) EYA2 ChIP-seq peaks in MDA-MB-231 cells by genomic features.

(B) ChIP analysis of Flag-EYA2 or Flag-EYA2-2A binding the *Gas6* promoter in MDA-MB-231 cells (n = 3). GAPDH, control. ChIP performed with anti-Flag antibody. IgG, IP control.

(C) ChIP analysis of Flag-FBXO7 binding to *Gas6* promoter in MDA-MB-231 cells (n = 3). GAPDH, control. ChIP performed with anti-Flag antibody. IgG, IP control.

(D) ChIP analysis of Flag-EYA2 binding the *Gas6* promoter in MDA-MB-231 cells expressing FBXO7 or Δ F-FBXO7 (n = 3). GAPDH, control. ChIP performed with anti-Flag antibody. IgG, IP control.

(E and F) RT-qPCR analysis of GAS6 in MCF7 cells transfected with the indicated vectors (n = 3).

(G) Immunoblots of AXL signaling proteins in control or FBXO7 KD MDA-MB-231 cells transfected with control or FBXW7 siRNAs. GAPDH, loading control.

(H) Flow cytometry analysis of HLA-A/B/C surface expression on control, FBXO7 KD, and FBXO7 KD + GAS6 MDA-MB-231 cells.

Data represent mean \pm SEM. ns, not significant; **p < 0.01; ****p < 0.0001 by one-way ANOVA followed by Dunnett's multiple comparisons test (E and F), two-way ANOVA followed by Tukey's multiple comparisons test (B and D), and Sidak's multiple comparisons test (C).

Figure S5

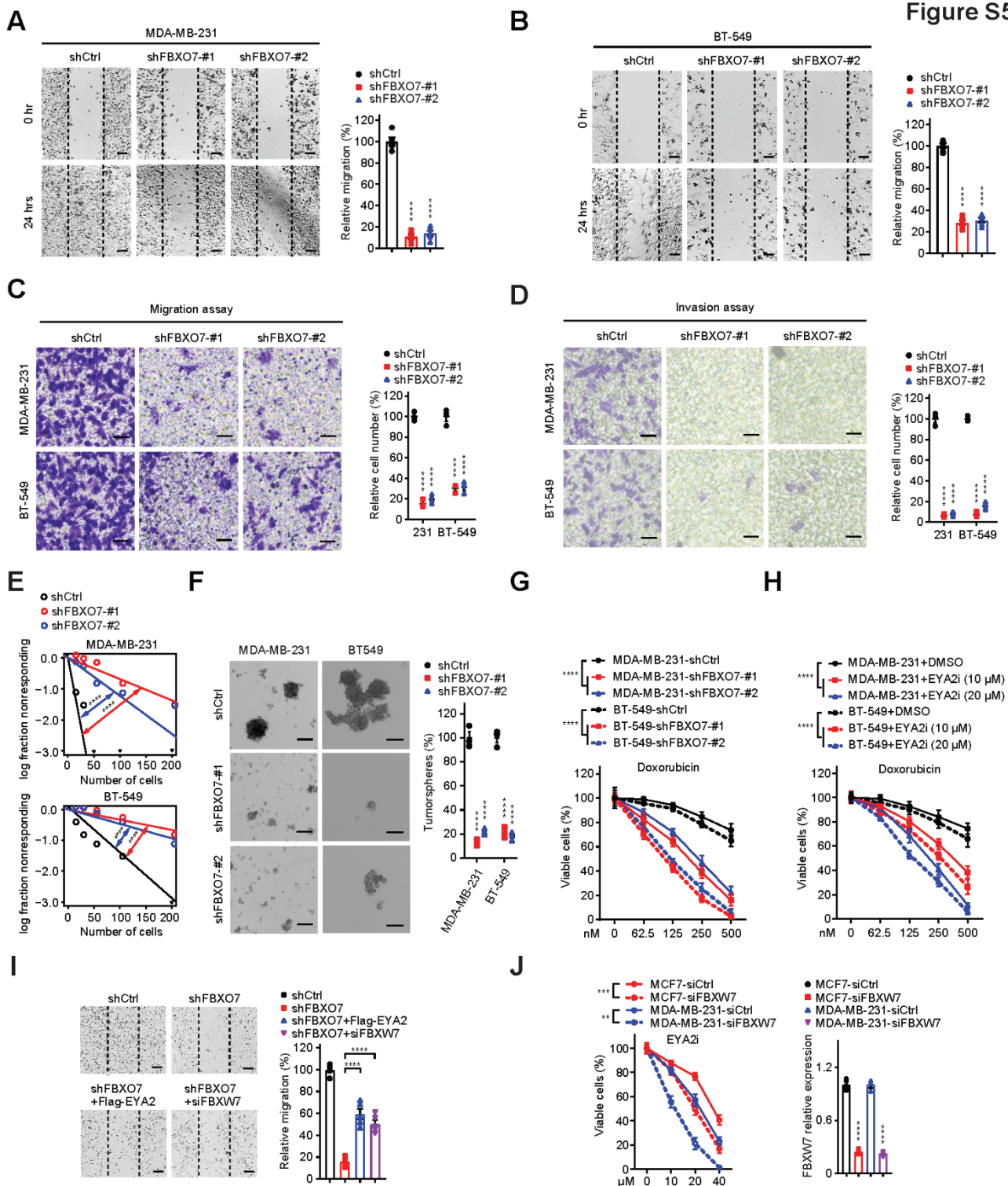


Figure S5. Targeting FBXO7/EYA2 decreases mesenchymal-associated phenotypes of cancer cells *in vitro*, related to Figure 5.

(A and B) Gap closure assays of control and FBXO7 KD MDA-MB-231 (A) and BT-549 (B) cells (left panels). Quantification of migration (right panels). Five fields were randomly chosen and quantified (n = 5).

(C and D) Boyden chamber assays of migration (C) and invasion (D) for the indicated control and FBXO7 KD cells (left panels). Quantification of data (right panels). Three fields were randomly chosen and quantified (n = 3).

(E) ELDA for indicated control and FBXO7 KD cells (n = 3).

(F) Representative images (left panels) and quantification (right panel) of tumorspheres of the indicated control and FBXO7 KD cells (n = 3). Scale bar, 50 μ m.

(G and H) Viabilities of the indicated cells expressing control or FBXO7 shRNA (G) or treated with vehicle or EYA2i (H) upon doxorubicin treatment for 72 hrs (n = 3).

(I) Gap closure assays of control or FBXO7 KD MDA-MB-231 cells expressing Flag-EYA2 or transfected with FBXW7 siRNA (left panels). Quantification of migration (right panel). Five fields were randomly chosen and quantified (n = 5).

(J) Viabilities of the indicated control and FBXW7 KD cells treated with EYA2i (left panel). RT-qPCR analysis of FBXW7 (right panel) (n = 3).

Data represent mean \pm SEM. **p < 0.01; ***p < 0.001; ****p < 0.0001 by one-way ANOVA followed by Dunnett's multiple comparisons test (A and B), Tukey's multiple comparisons test (I; J, right panel), two-way ANOVA followed by Dunnett's multiple comparisons test (C and D), Tukey's multiple comparisons test (F, G, H; J, left panel), and χ^2 test for pair-wise differences (E).

Figure S6

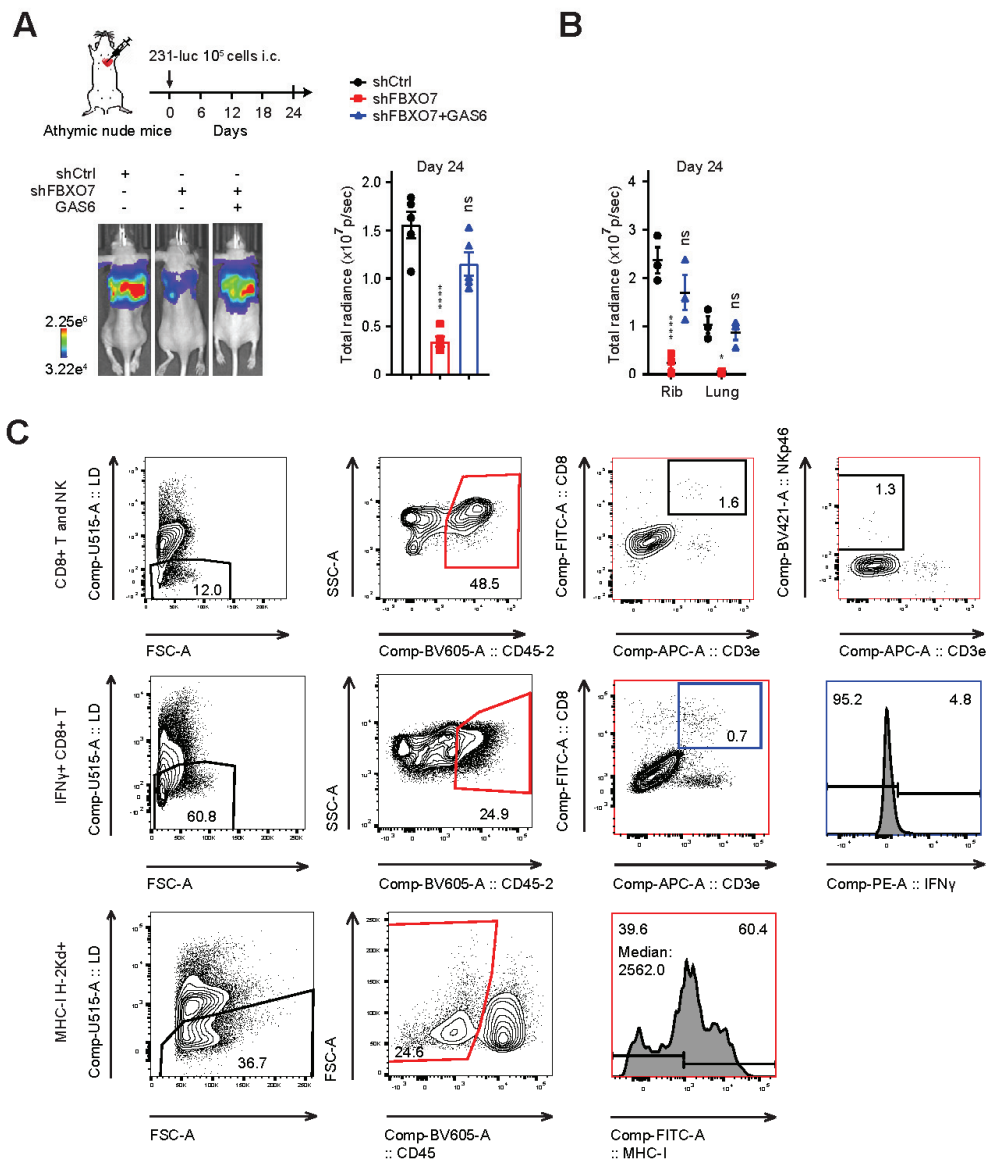


Figure S6. FBXO7/EYA2 inhibition attenuates tumor growth, boosts antitumor immunity, and enhances ICB therapy response, related to Figure 6.

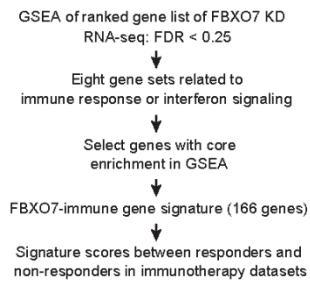
(A and B) Representative bioluminescence images of immunocompromised mice 24 days post-intracardiac injection with control, FBXO7 KD, and FBXO7 KD + GAS6 MDA-MB-231-*luc* cells (A, bottom left panel). Schematic of injection (A, top left panel). Plot of total body radiance (A, right panel) (n = 5). Plot of organ radiance (B) (n = 3).

(C) Flow cytometry gating strategies for detection of tumor-infiltrating CD8⁺ T and NK cells (top panels), IFN γ ⁺CD8⁺ T cells (middle panels), and MHC-I H-2Kd⁺ 4T1-*luc* tumor cells (bottom panels).

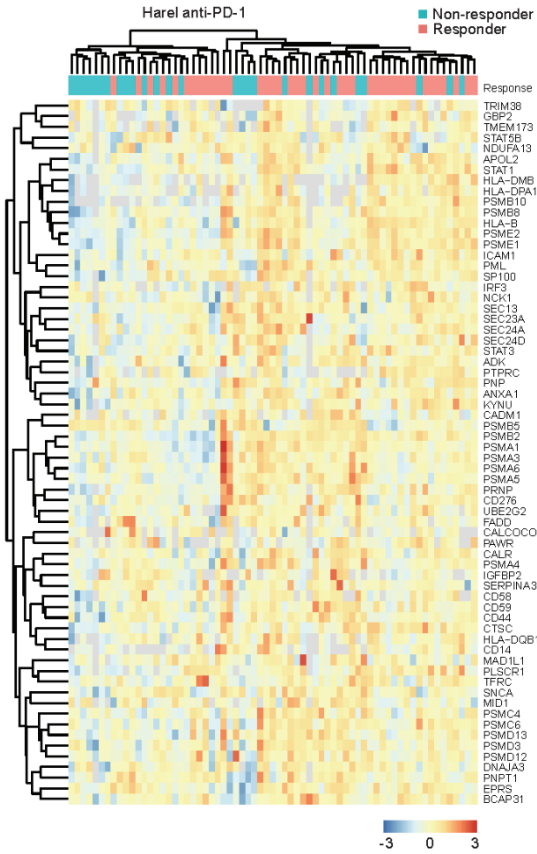
Data represent mean \pm SEM. ns, not significant; *p < 0.05; ****p < 0.0001 by one-way ANOVA followed by Tukey's multiple comparisons test (A), and Tukey's multiple comparisons test (B).

Figure S7

A



B



C

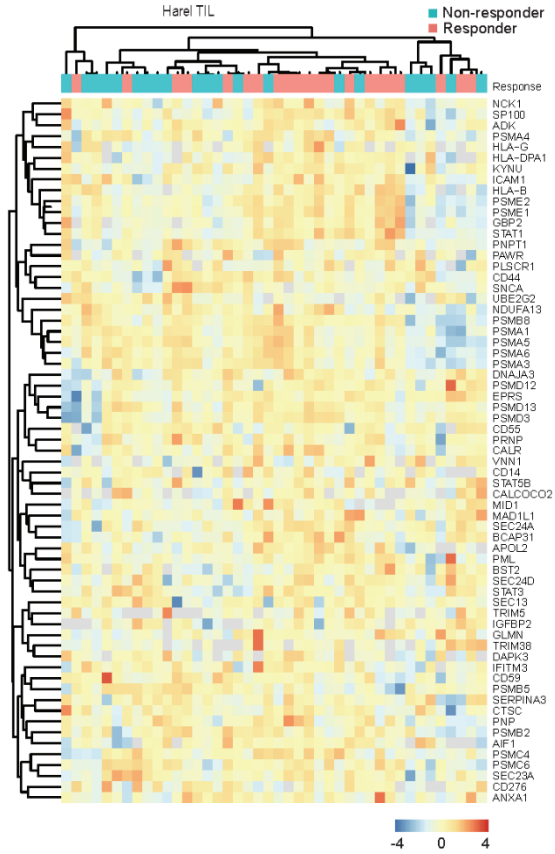


Figure S7. FBXO7 associates with mesenchymal and immune-suppressive phenotypes in cancer patient datasets, related to Figure 7.

(A) Generation of FBXO7-immune gene signature (166 immune-related genes) based on GSEA analysis of FBXO7 KD RNA-seq data.

(B and C) Heatmaps of FBXO7-immune gene signature differentially enriched in “responder” versus “non-responder” patients in Harel anti-PD-1 (B) and Harel TIL therapies (C) datasets.